Supporting Information for

Porous electrospun fibers embedding TiO$_2$ for adsorption and photocatalytic degradation of water pollutants

Chang-Gu Lee[a,b], Hassan Javed[a,b], Danning Zhang[a,b], Jae-Hong Kim[a,c], Paul Westerhoff[a,d],

Qilin Li[a,b], and Pedro J.J. Alvarez[a,b*]

[a] *NSF Nanosystems Engineering Research Center for Nanotechnology Enabled Water Treatment (NEWT)*

[b] *Dept. of Civil and Environmental Engineering, Rice University, Houston, TX 77005*

[c] *Dept. of Chemical and Environmental Engineering, Yale University, New Haven, CT 06511*

[d] *School of Sustainable Engineering and the Built Environment, Arizona State University, Tempe, AZ 85287*

* Department of Civil and Environmental Engineering, Rice University, Houston, Texas 77005, United States. Tel.: +1 713 348 5903.
 E-mail: alvarez@rice.edu (P.J.J. Alvarez)

Number of pages:	**23**
Number of Figures:	**16**
Number of Tables:	**3**

Thermal Properties and nTiO₂ Content

The thermal degradation experiment were conducted to determine the $nTiO_2$ loading contents on the sample mats. TGA thermograms of the pristine PVDF mat (EF) and the other mats (EF-TiO_2, EPF(2/1)-TiO_2, EPF(1/1)-TiO_2) that had $nTiO_2$ nanopowder were shown in Figure S1. The onset degradation temperature, which is the intersection of the tangent line at the steepest part of the mass decomposition curve and the extension line of the pre-decomposition part, was 451.63°C for EF. It was higher than the decomposition temperature of the PVDF supplied by the vendor (>315°C) due to the higher crystallinity coming from the fabricate procedure.[1,2] But, the onset degradation temperature was decreased after incorporation of TiO_2 in the order of EPF(2/1)-TiO_2 (396.34°C), EPF(1/1)-TiO_2 (380.98°C), and EF-TiO_2 (325.63°C). Ramasundaram et al. showed similar results in the case of $nTiO_2$ electrospraying onto the PVDF nanofiber mat, meanwhile Vild et al. reported the increase of thermal stability after incorporation of TiO_2 into the poly(methyl methacrylate) (PMMA) electrospun nanocomposite.[1,3] Therefore, this indicates that the thermal stability of the photocatalytic composite is affected not only by the photocatalyst contents but also by the support properties. Based on the difference in the residual weight ratio of the pristine PVDF mat (EF: 22.53%), the $nTiO_2$ loading contents was estimated and represented in Table 1.
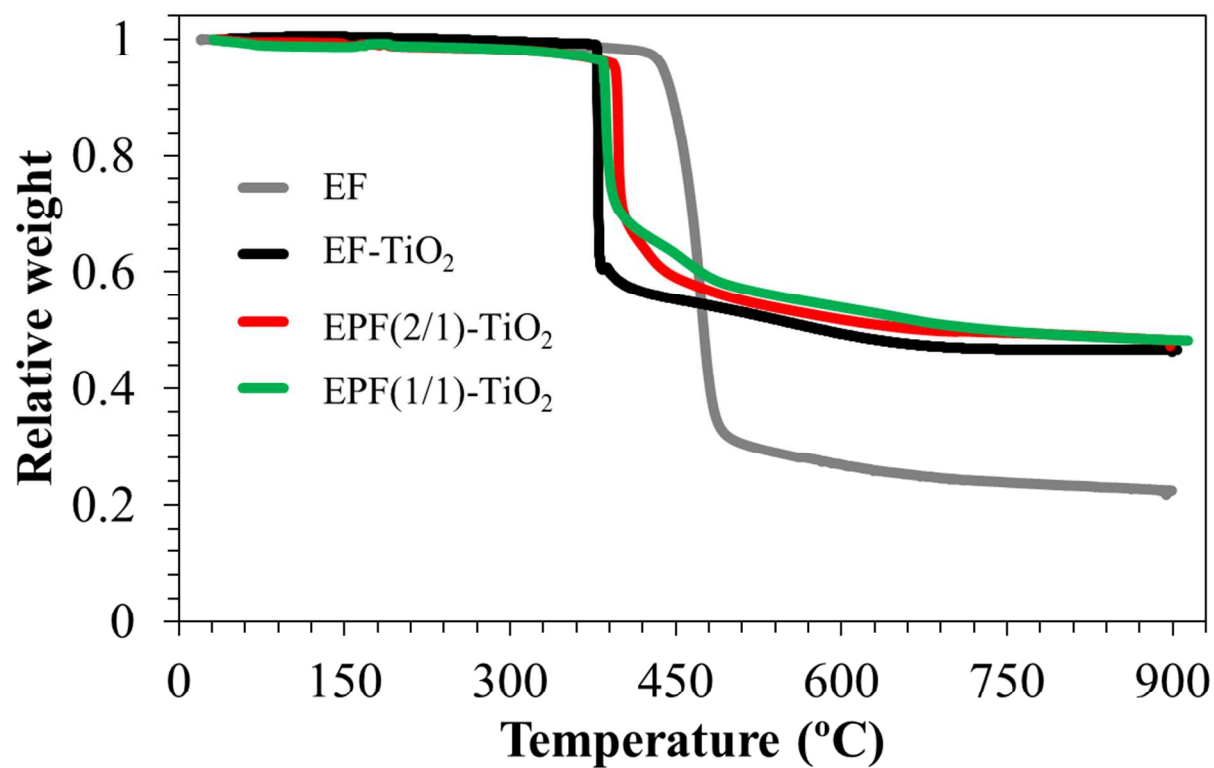
Figure S1. Thermogravimetric Analysis (TGA**)** thermograms of the fabricated mat samples (EF: PVDF(18%), EF-TiO$_2$: PVDF(18%)-TiO$_2$, EPF(2/1)-TiO$_2$: PVDF(12%)/PVP(6%)-TiO$_2$ with washing, EPF(1/1)-TiO$_2$: PVDF(9%)/PVP(9%)-TiO$_2$).
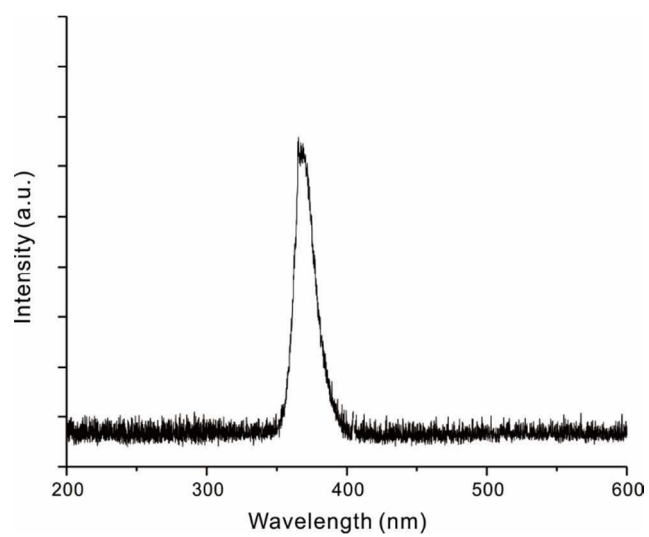
Figure S2. Wave length spectrum of UVA lamps.

Chemical Actinometry

Potassium ferrioxalate method as a chemical actinometry was applied for estimation of light intensity inside of the quartz beaker.[4, 5] Prior to analysis, 0.2 M ferric sulfate solution in 2 N H_2SO_4 (Sol A), 1.2 M potassium oxalate solution (Sol B), 0.6 M sodium acetate buffer solution at pH 4.5 (Sol C), 0.2% 1,10-phenanthroline solution (Sol D), 2 N H_2SO_4 solution (Sol E), and 0.4 mM $FeSO_4$ in 0.1 N H_2SO_4 (Sol F) were prepared, separately. To make a standard curve of ferrous iron, 0 to 3 ml of Sol F were added into the 10 ml volumetric flasks with 2 ml of Sol C and 2 ml of Sol D. Deionized water (DI) was added to the 10 mL mark and put in a dark for 40 min. Then, the absorbance of solution were measured using a quartz cuvette at 510 nm. Potassium ferrioxalate solution was prepared as follows in 1 L volumetric flask. 15.2 mL of Sol B was mixed with about 800 ml of DI. Then, 35 ml of Sol E and 6 ml of Sol A were added sequentially, and DI added up to the 1 L mark. The solution was poured into the quartz beaker (50 ml) and placed in the photo-reactor. Sampling were performed over time from photo-reactor and the concentration of ferrous iron generated during reaction was determined via calibration curve (Figure S3). The light intensity (*I*) was calculated by the following equation:

$$I = \Delta n/(10^{-3} \cdot \Phi \cdot V \cdot t) \quad (unit: Einstein/cm^2/s) \qquad \text{(Eq. S1)}$$

Where *Δn* is ferrous iron photo-generated (mole), *Φ* is quantum yield (1.22 for UV light centered at 350 nm), *V* is irradiated volume (ml), and *t* is irradiation time (s). All experiments must be performed in the dark room, only the red lamp is allowed as an illumination. During 180 s of irradiation time, 5.76×10^{-5} moles of ferrous iron were generated in the quartz beaker (50 ml, 72.02 cm^2), which yields 3.64×10^{-9} einstein/cm^2/s of the light intensity (*I*).
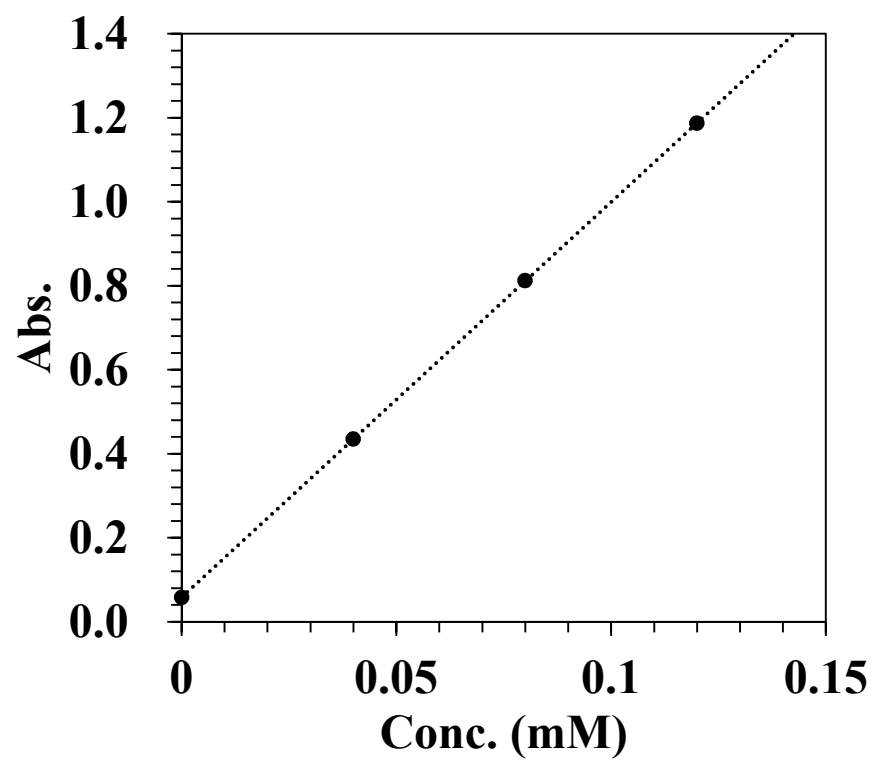
Figure S3. Standard curve of ferrous iron concentration versus the absorbance at 510 nm.

Table S1. Water quality data of the secondary effluent from a wastewater treatment plant in Houston, TX (i.e., West University Place WWTP).

TOC[†]	pH	DO[††]	TSS[†††]	Conductivity	UV$_{254}$[††††]
(mg/L)	(-)	(mg/L)	(mg/L)	(μS/cm)	(-)
17.11 ± 0.23	6.99 ± 0.01	6.89 ± 0.31	42.50 ± 10.61	770.70 ± 0.10	0.156 ± 0.001

[†] TOC: total organic carbon

[††] DO: dissolved oxygen

[†††] TSS: total suspended solid

[††††] UV$_{254}$: UV-absorbance at 254 nm

Table S2. Physical and chemical characterization of TiO$_2$ slurry.

BET specific surface area	Total pore volume	Zeta potential in DI[†]	Zeta potential in WWE[††]	Hydrodynamic diameter in DI	Hydrodynamic diameter in WWE
(m^2/g)	(cc/g)	(mV)	(mV)	(nm)	(nm)
61.82	1.13	-37.86 ± 2.25	-16.97 ± 1.47	228.83 ± 26.79	457.11 ± 41.46

[†] DI: deionized water
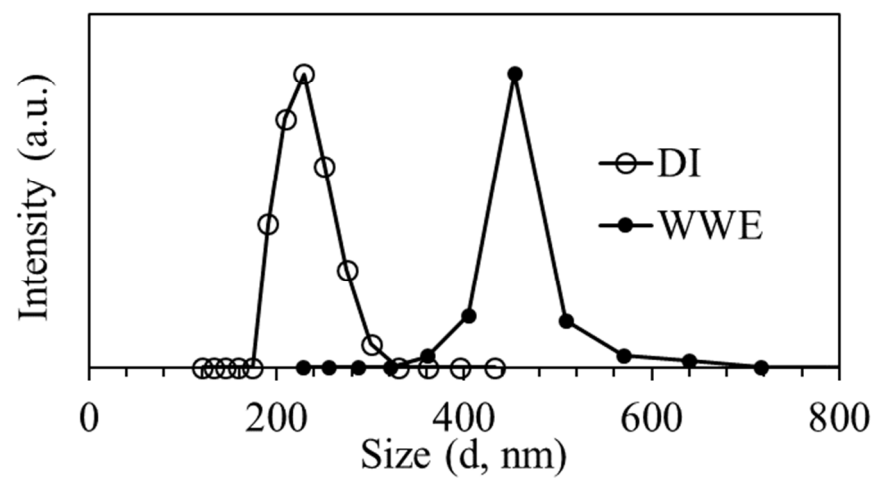
[††] WWE: wastewater effluent

Figure S4. Size distribution of TiO$_2$ slurry based on dynamic light scattering (DLS) data in deionized water (DI) and wastewater effluent (WWE).
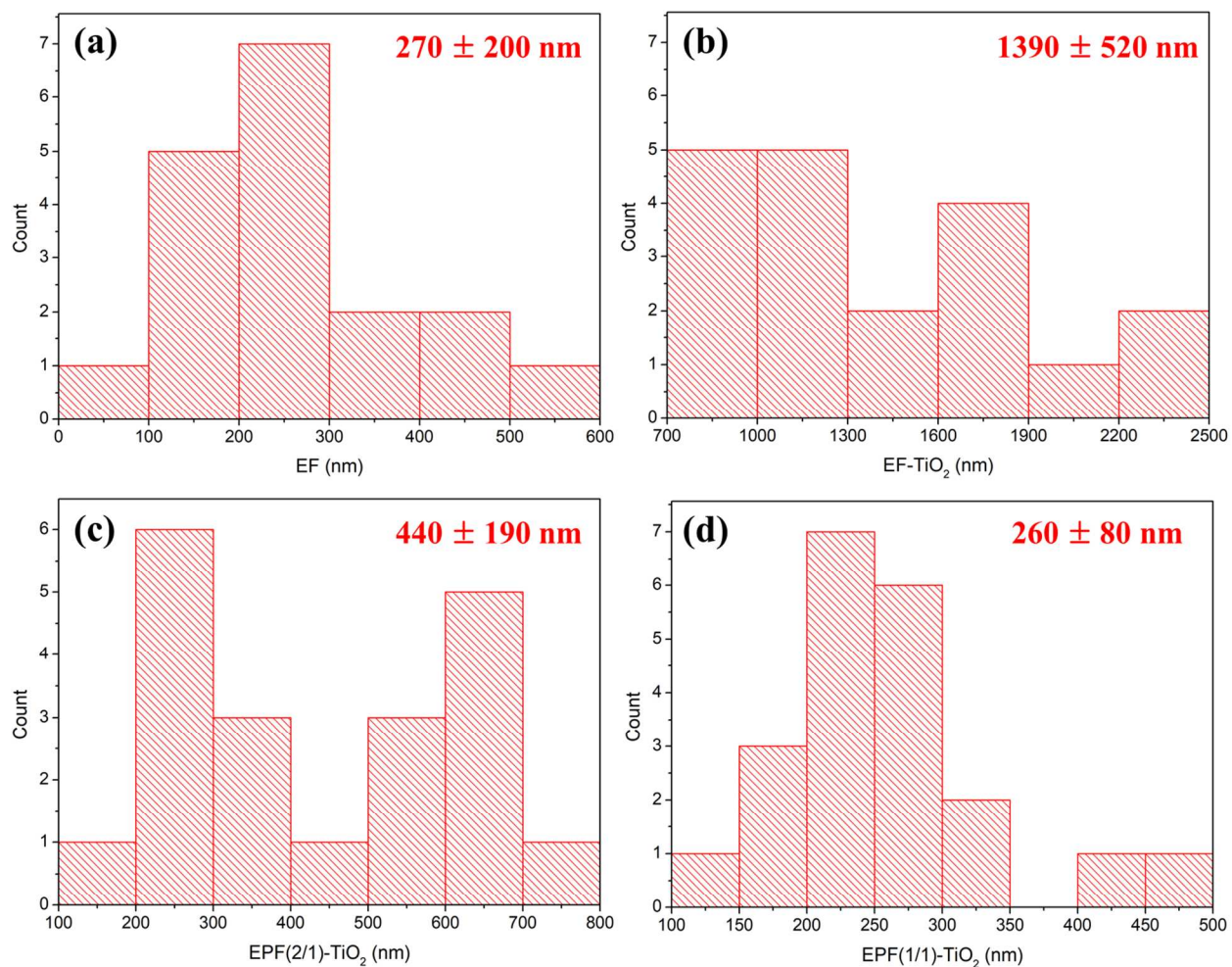
Figure S5. Electrospun fiber diameter analysis of (a) EF: PVDF(18%), (b) EF-TiO$_2$: PVDF(18%)-TiO$_2$, (c) EPF(2/1)-TiO$_2$: PVDF(12%)/PVP(6%)-TiO$_2$, and (d) EPF(1/1)-TiO$_2$: PVDF(9%)/PVP(9%)-TiO$_2$.
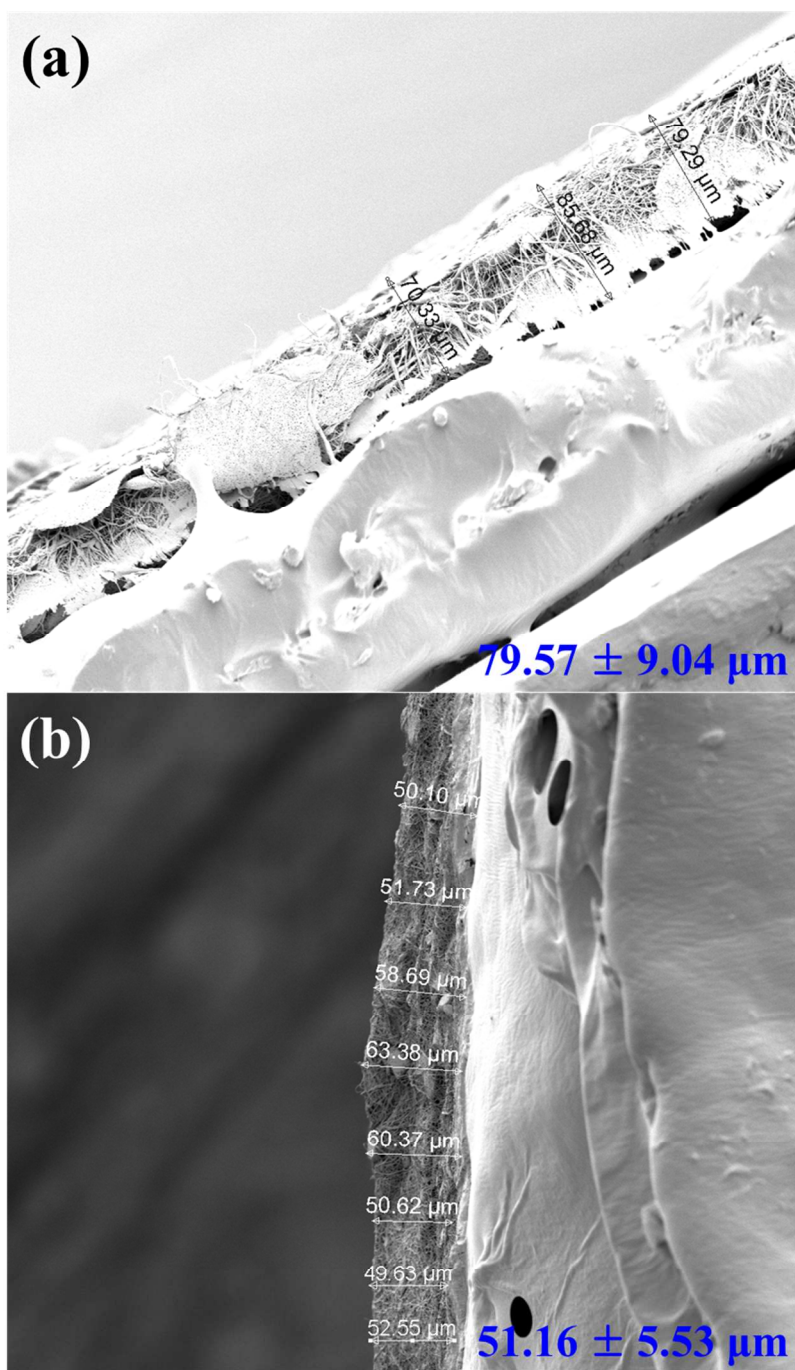
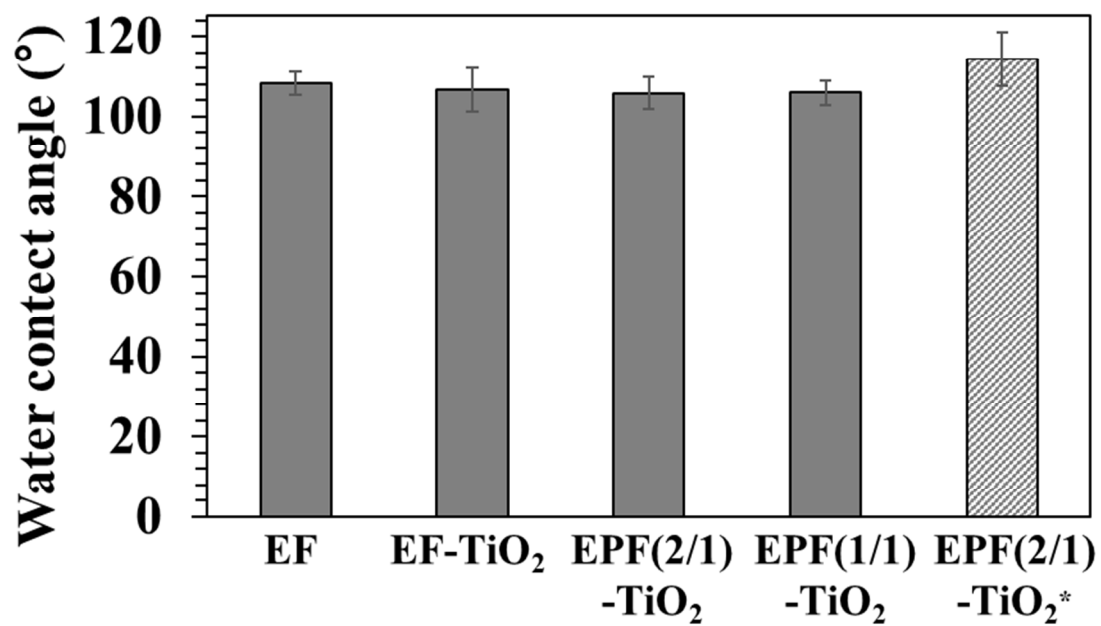**Figure S6.** Cross section SEM image of (a) EPF(2/1)-TiO$_2$ mat and (b) EPF(1/1)-TiO$_2$ showing mat thickness.

Figure S7. Water contact angle of the samples (EF: PVDF(18%), EF-TiO$_2$: PVDF(18%)-TiO$_2$, EPF(2/1)-TiO$_2$: PVDF(12%)/PVP(6%)-TiO$_2$, and EPF(1/1)-TiO$_2$: PVDF(9%)/PVP(9%)-TiO$_2$). (* after photocatalytic degradation by UVA irradiation)
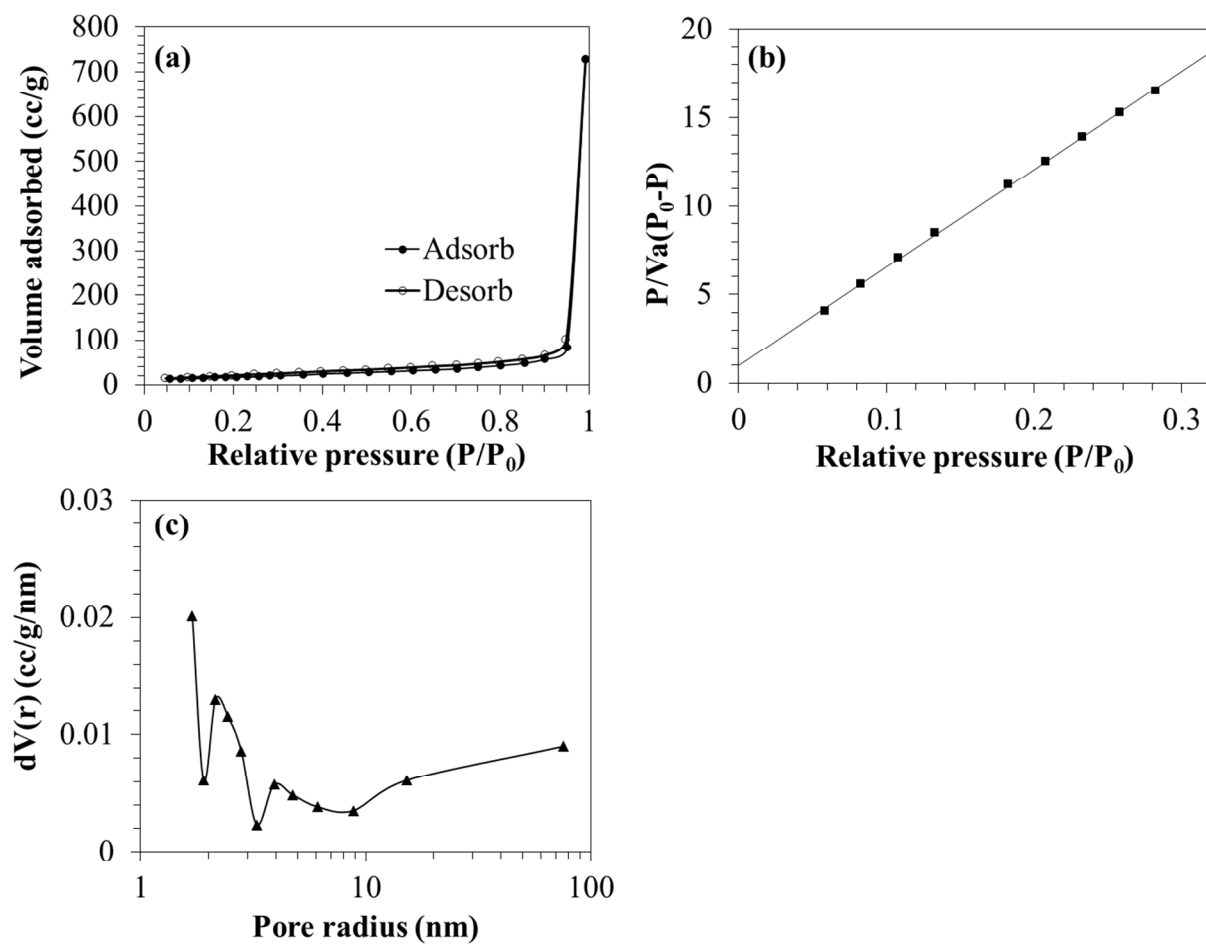
Figure S8. Surface area analysis and pore size distribution of TiO_2 nanopowder: (a) N_2 adsorption-desorption curves; (b) BET surface analysis; (c) BJH pore distribution.
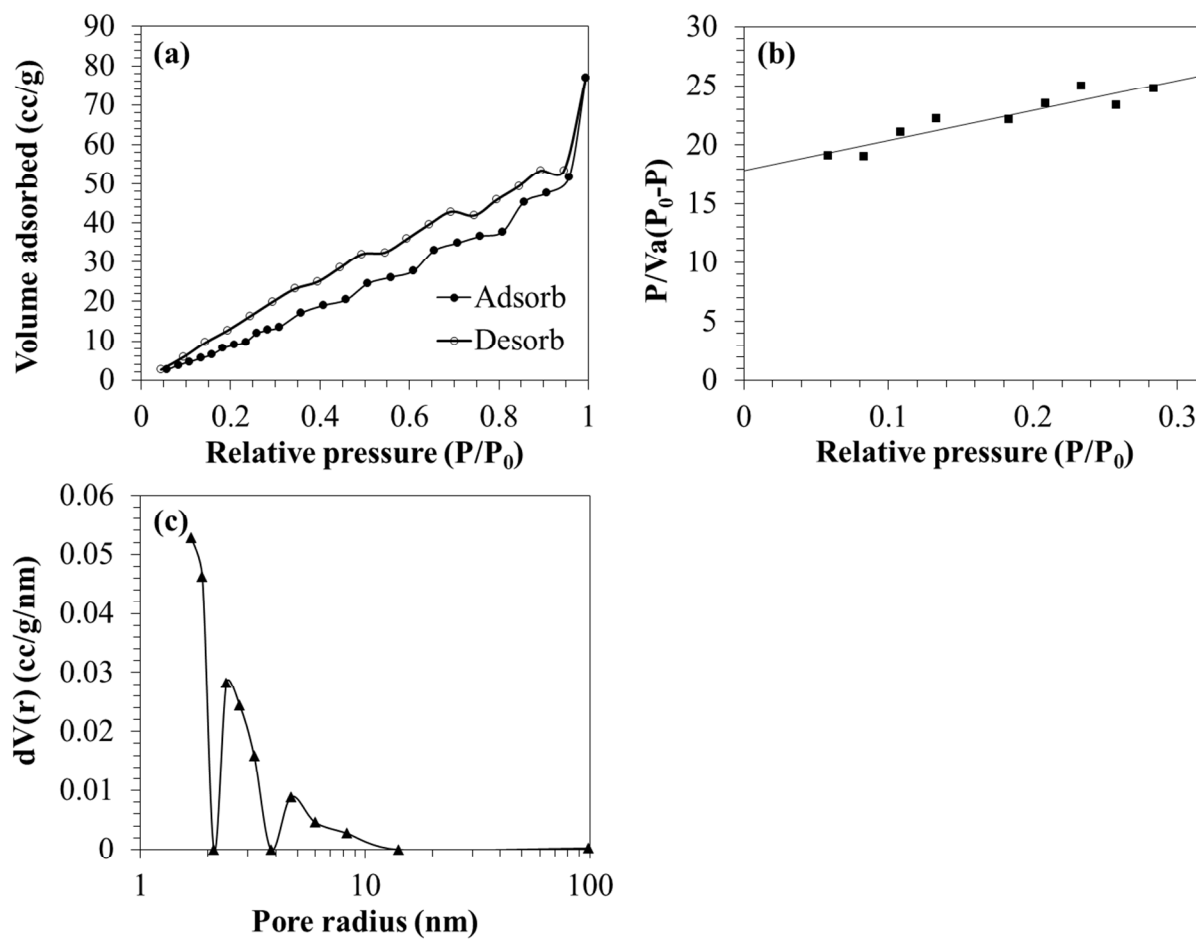
Figure S9. Surface area analysis and pore size distribution of EF: (a) N_2 adsorption-desorption curves; (b) BET surface analysis; (c) BJH pore distribution.
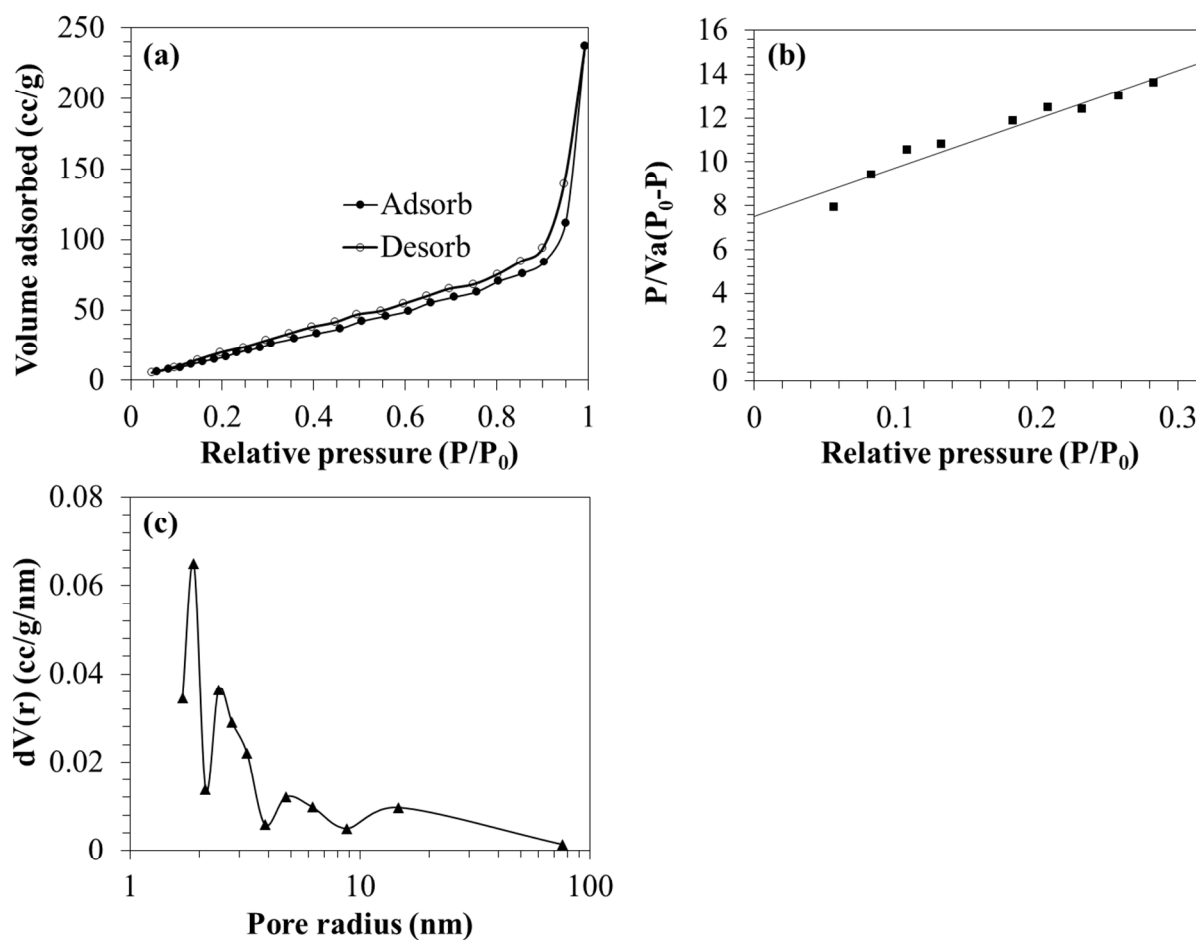
Figure S10. Surface area analysis and pore size distribution of EPF(2/1)-TiO$_2$: (a) N$_2$ adsorption-desorption curves; (b) BET surface analysis; (c) BJH pore distribution.

Figure S11. Surface area analysis and pore size distribution of EPF(1/1)-TiO$_2$: (a) N$_2$ adsorption-desorption curves; (b) BET surface analysis; (c) BJH pore distribution.
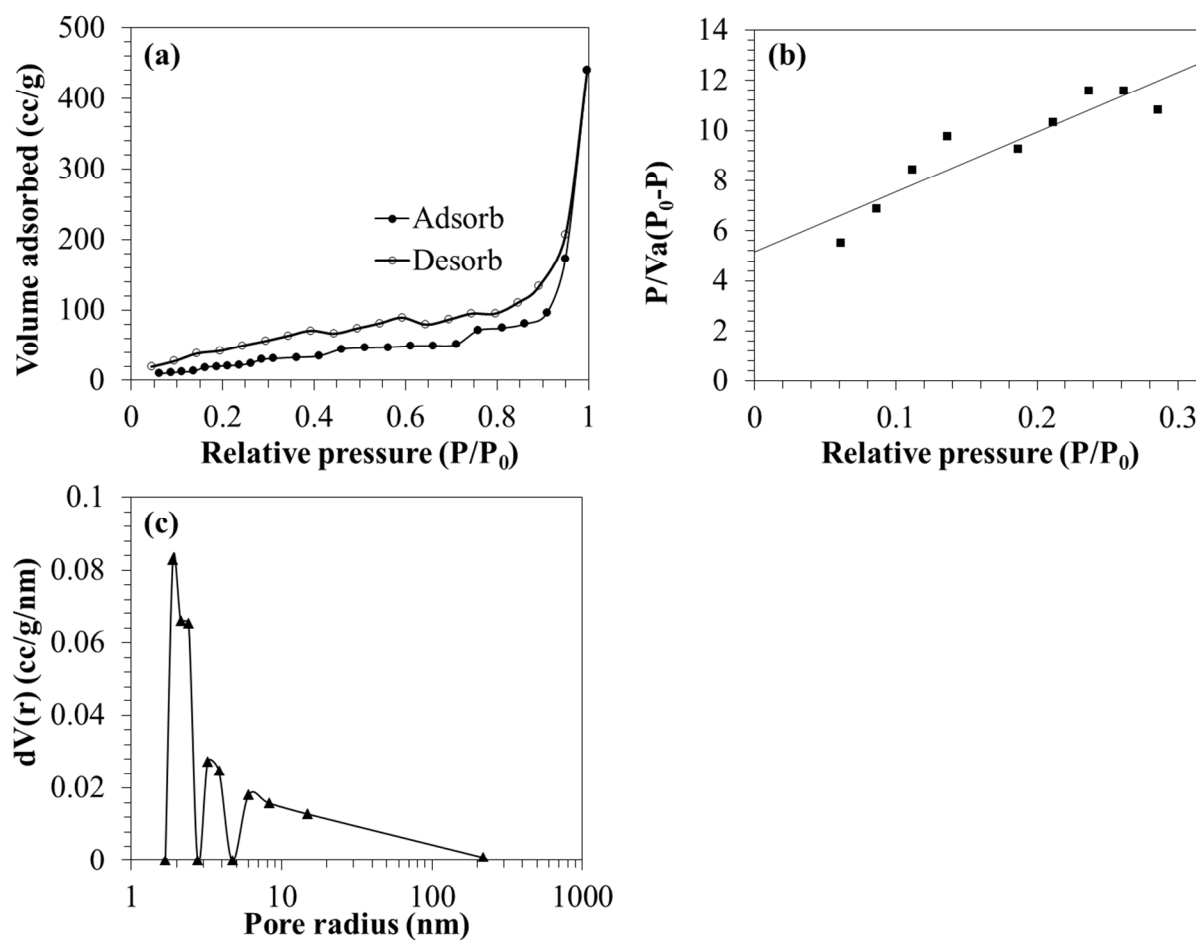
Adsorption Capacity for Contaminants

The adsorption capacity of restored EPF(2/1)-TiO$_2$ sample were evaluated at different concentration of contaminants (methylene blue (MB), bisphenol A (BPA), and 17α-ethynylestradiol (EE2)). The equilibrium concentrations were used for the following Langmuir (Eq. S2) and Freundlich (Eq. S3) isotherm model analysis.

$$q_e = \frac{Q_m K_L C_e}{1 + K_L C_e}$$
(Eq. S2)

$$q_e = K_F C_e^{\frac{1}{n}}$$
(Eq. S3)

where q_e and C_e are the amount of MB adsorbed on the sample mat and MB concentration in the aqueous solution at equilibrium, respectively. Q_m is the maximum adsorption capacity, K_L is the Langmuir constant related to the binding site affinity, K_F is the Freundlich constant related to the adsorption capacity, and $1/n$ is the Freundlich constant related to the adsorption intensity. As shown in Figure S13, the equilibrium adsorption data were better fitted by Langmuir isotherm that assumes uniform monlolayer adsorption.[6] The isotherm model parameters were represented in Table S3.
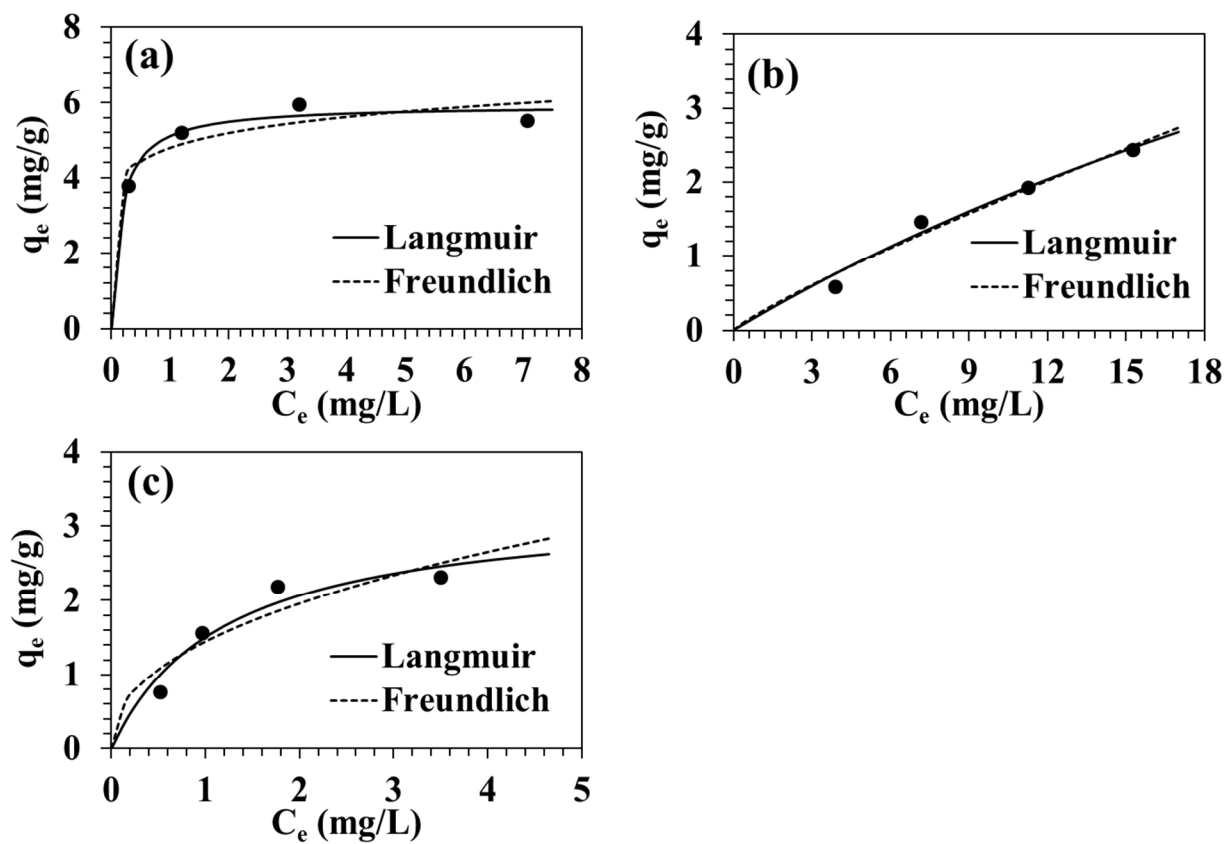
Figure S12. Isotherm model fitting for (a) methylene blue (MB), (b) bisphenol A (BPA), and (c)

17α-ethynylestradiol (EE2).

Table S3. Isotherm parameters for the adsorption of contaminants on the EPF(2/1)-TiO$_2$ mat.

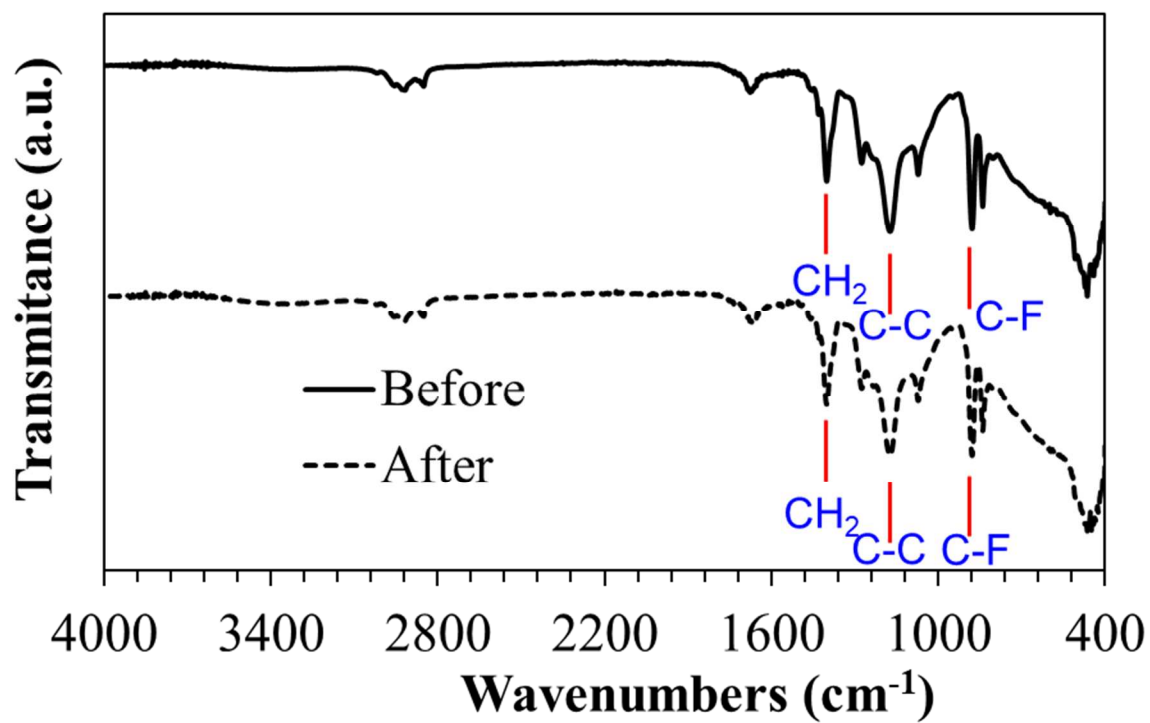| | Langmuir | | | | Freundlich | | | |
	Q_m	K_L	R^2	SSE[†]	K_F	$1/n$	R^2	SSE[†]
	(mg/g)	(L/mg)	(-)	(-)	(L/g)	(-)	(-)	(-)
MB	5.93 ± 0.23	6.19 ± 1.60	0.94	0.17	4.79 ± 0.34	0.11 ± 0.05	0.74	0.69
BPA	10.80 ± 8.52	0.02 ± 0.02	0.98	0.05	0.23 ± 0.08	0.87 ± 0.14	0.97	0.06
EE2	3.29 ± 0.65	0.85 ± 0.42	0.92	0.13	1.45 ± 0.22	0.44 ± 0.16	0.83	0.26

[†] SSE: sum of squared errors

Figure S13. FT-IR spectrum of EPF(2/1)-TiO$_2$ before using photocatalytic oxidation and after 10 reusing photocatalytic oxidation.
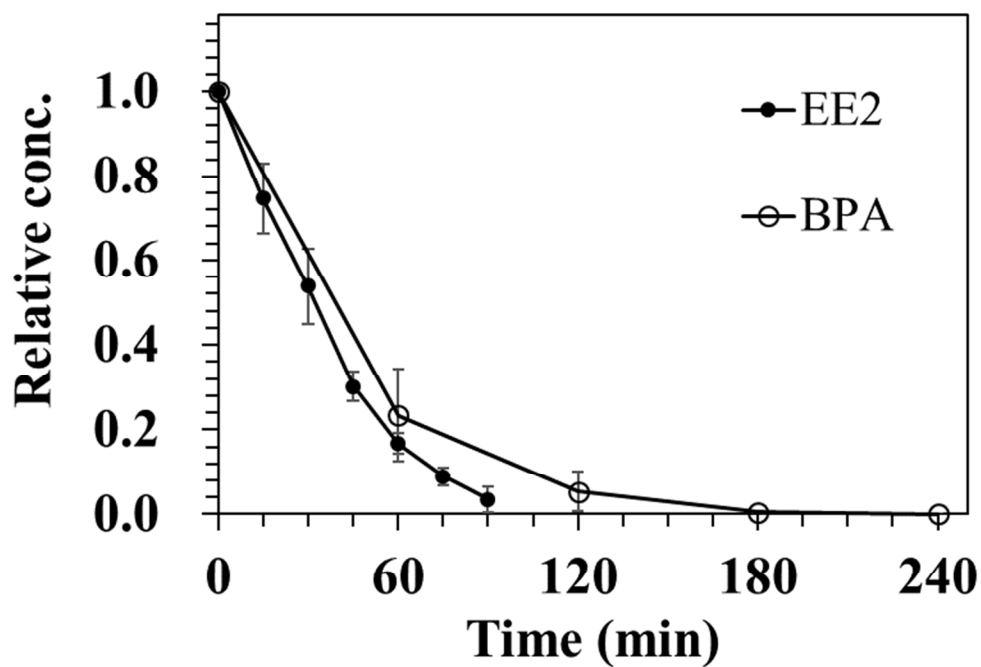
Figure S14. Removal of 17α-ethynylestradiol (EE2) and bisphenol A (BPA) in DI water under UVA irradiation (3.64×10^{-9} einstein/cm^2/s) using electrospun porous fiber photocatalytic mat containing nTiO$_2$ (EPF(2/1)-TiO$_2$) ($C_0 = 5$ mg/L).
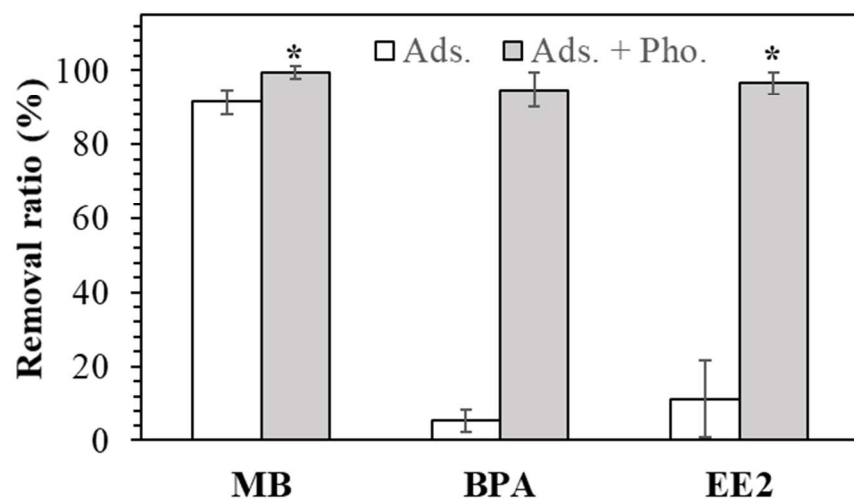
Figure S15. Removal of various pollutants by the photocatalytic mat (EPF(2/1)-TiO$_2$) by adsorption under dark conditions (Ads.) versus concurrent degradation under UVA irradiation (Ads. + Pho.). Initial concentrations were 3.2 mg/L for methylene blue (MB), 5 mg/L for bisphenol A (BBA), and 5 mg/L for 17α-ethynylestradiol (EE2). All tests were conducted for 2 h except (˙) for photocatalytic degradation of MB and EE2 (1.5 h).
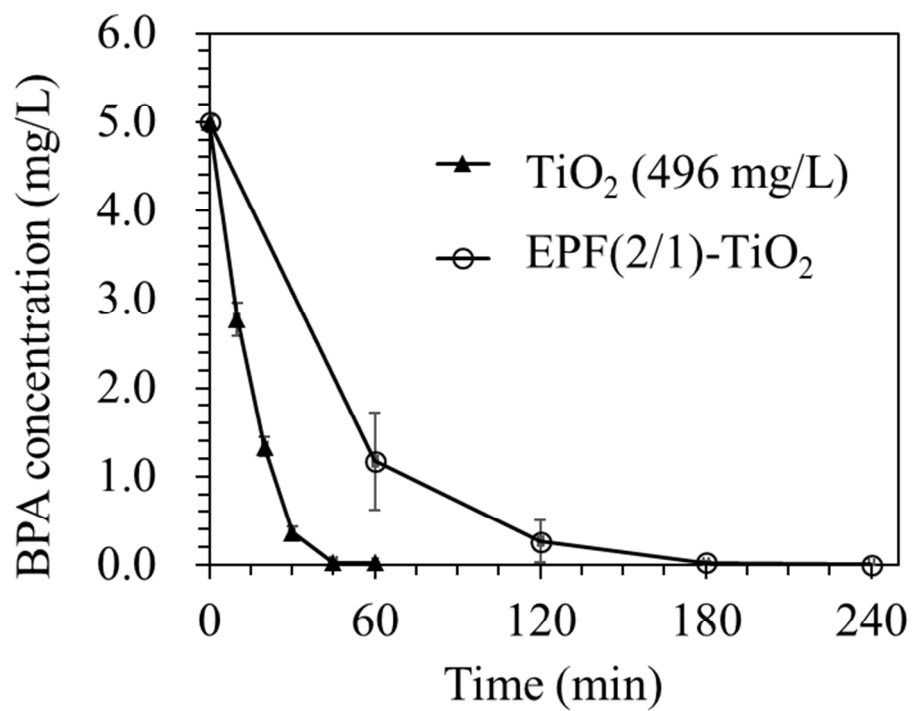
Figure S16. Bisphenol A removal (C_0 = 5 mg/L) in DI water under UVA irradiation (3.64×10^{-9} einstein/cm^2/s) using a photocatalytic mat (EPF(2/1)-TiO$_2$) versus nTiO$_2$ slurry at an equivalent concentration (496 mg/L). The data show loss of activity upon nTiO$_2$ immobilization.

References

1. Ramasundaram, S.; Son, A.; Seid, M. G.; Shim, S.; Lee, S. H.; Chung, Y. C.; Lee, C.; Lee, J.; Hong, S. W., Photocatalytic applications of paper-like poly(vinylidene fluoride)-titanium dioxide hybrids fabricated using a combination of electrospinning and electrospraying. *J Hazard Mater* **2015,** *285*, 267-76.

2. Nasir, M.; Matsumoto, H.; Minagawa, M.; Tanioka, A.; Danno, T.; Horibe, H., Preparation of Porous PVDF Nanofiber from PVDF/PVP Blend by Electrospray Deposition. *Polymer Journal* **2007,** *39*, (10), 1060-1064.

3. Vild, A.; Teixeira, S.; Kühn, K.; Cuniberti, G.; Sencadas, V., Orthogonal experimental design of titanium dioxide—Poly(methyl methacrylate) electrospun nanocomposite membranes for photocatalytic applications. *Journal of Environmental Chemical Engineering* **2016,** *4*, (3), 3151-3158.

4. Bolton, J. R.; Stefan, M. I.; Shaw, P.-S.; Lykke, K. R., Determination of the quantum yields of the potassium ferrioxalate and potassium iodide–iodate actinometers and a method for the calibration of radiometer detectors. *Journal of Photochemistry and Photobiology A: Chemistry* **2011,** *222*, (1), 166-169.

5. Tugaoen, H. O. N. Photocatalysis for Reductive Transformation of Nitrate and Chromate in Drinking Water. Arizona State University, 2017.

6. Liu, X.; Jin, A.; Jia, Y.; Xia, T.; Deng, C.; Zhu, M.; Chen, C.; Chen, X., Synergy of adsorption and visible-light photocatalytic degradation of methylene blue by a bifunctional Z-scheme heterojunction of WO 3 /g-C 3 N 4. *Applied Surface Science* **2017,** *405*, 359-371.